RSC Advances

PAPER

View Article Online
View Journal | View Issue

Cite this: *RSC Adv.*, 2022, **12**, 19686

One-step high-yield preparation of nitrogen- and sulfur-codoped carbon dots with applications in chromium(VI) and ascorbic acid detection†

Fanrong Meng,[ab] Haoran Xu,[a] Shuolin Wang,[a] Jingxian Wei,[a] Wengong Zhou,[a] Qiang Wang,[a] Peng Li,[a] Fangong Kong[a] and Yucang Zhang*[b]

Received 18th March 2022
Accepted 26th May 2022

DOI: 10.1039/d2ra01758j

rsc.li/rsc-advances

In this research, a nitrogen- (N) and sulfur- (S) codoped carbon dot (CDs-IPM)-based sensor was synthesized using a single-step hydrothermal method. Specifically, microcrystalline cellulose (MCC) was the main raw material, which was extracted from banana pseudo-stem-based waste, while autonomous sulfonic acid-functionalized ionic liquid (SO_3H-IL) and polyethylene glycol 400 (PEG 400) acted as the N, S dopant, and surface modifier, respectively. Comprehensive spectroscopic characterization of the synthesized CDs-IPM revealed the introduction of S, N atoms in the matrix with existence of surface oxygenic functional groups. The CDs-IPM possessed enhanced photoluminescence (PL) intensity, synthetic yield, and PL quantum yield (PLQY). Additionally, electron transfer between the CDs-IPM, hexavalent chromium (Cr(VI)), and subsequent ascorbic acid (AA) succeeded in turning the fluorescence on and off. The detection limit was 17 nM for Cr(VI), while it was 103 nM for AA. Our study data can simplify the process of synthesis of CDs utilizing biodegradable starting materials. The probe reported in this study may serve as a valuable addition to the field of environment monitoring by virtue of its enhanced detection sensitivity, high selectivity, and stability.

Introduction

Chromium(VI) [Cr(VI)] has been identified as an environmentally hazardous heavy metal ion which finds wide-scale industrial application in ore smelting, leather tanning, dyeing, and metal electroplating.[1] The side-effects of Cr(VI) exposure include liver and kidney damage, and increased risk of cancer. As such, Cr(VI) contamination and its detection in natural water bodies and soil have drawn extensive attention. In this review, the development of cost-effective detection methods for Cr(VI) is becoming increasingly important. Nowadays, nanomaterials have received great interest due to their broad application prospects in environmental remediation.[2–4] In particular, carbon nanodots (CDs) have been established as a versatile fluorescent sensor readily used for efficient metal ion recognition.[5–7]

As a photoluminescent nanomaterial, CDs have generated extensive interest due to their widespread application in the fields of sensing,[8] optoelectronic devices,[9] anti-counterfeit detection,[10,11] clinical therapy,[12–14] and energy production.[15] Different top-down and bottom-up synthetic methods have been exploited in order to fabricate CDs by adopting various molecular precursors or biomass with different sources.[16] As one of the wet-chemistry-based bottom-up methods, the hydrothermal carbonization technique is by far an efficient method since it is relatively straightforward and cost-effective. Natural bioresources such as coffee grounds,[17] olive solid wastes,[18] denatured milk,[19] fresh aloe,[20] and water hyacinth[21] are increasingly being reported as viable carbon sources replacing their predecessor toxic precursors. Banana Pseudo-stem (BPs), a by-product obtained after the banana harvested, is mainly composed of cellulose, hemicellulose and lignin.[22] Large amount of BPs discarded every year offer an ideal opportunity for extracting value-added cellulose and producing CDs.

Although, techniques using bioresources as raw materials for synthesis are practical and economical, the bio-based CDs mostly used for fluorescence sensors have relatively low yield or have undesirable photoluminescence quantum yield (PLQY). The three experimental methods for synthesizing CDs with high PLQY involve the incorporation of heteroatoms,[23] surface modification/passivation by polymeric materials,[24] and host–guest assembly by porous materials,[25] respectively. Among these three existing methods, doping modification is widely perceived as an effective way to improve the properties of functional nano materials.[26–29] Heteroatom (*e.g.*, nitrogen, sulfur, phosphorus, boron, chlorine, copper, zinc, iron, *etc.*) doping is the most efficient means to improve fluorescence efficiency which enhances

[a]*State Key Laboratory of Biobased Material and Green Papermaking, Qilu University of Technology (Shandong Academy of Sciences), Jinan, 250353, P. R. China*
[b]*College of Food and Biological Engineering, Jimei University, Xiamen, 361021, P. R. China. E-mail: yczhang@jmu.edu.cn*

† Electronic supplementary information (ESI) available. See https://doi.org/10.1039/d2ra01758j

the electronic and optical performances of the carbon nanomaterials and improves their affinity to analytes *via* exposing sufficient active binding sites.[23] However, the systematic study of CDs synthesized employing hydrothermal methods is significantly astricted due to their transient physicochemical stability, which may be improved by surface functionalization. Despite the presence of functional molecule-based CDs surface passivation methods using diverse organic/inorganic molecules, polymers or ions,[14] the post-processing steps for surface modification are usually complicated due to its tedious purification procedure and long synthesis duration. The hassle-free and cost-effective chemical route for nanometer material synthesis has long been the pursuit of researchers.[30] Therefore, a single-step synthesis method of carbon dots with simultaneous impurity doping and surface passivation is worth exploring.

Ascorbic acid (AA), a water-soluble vitamin C, exists generally in pharmaceutical product, cosmetic formulations and human diet. AA has antioxidant properties and can prevent cardiovascular disease, cancer, and spiritual illnesses.[31] To this end, the determination of AA is of significance. Numerous methods for the determination of AA have been applied, including electrochemistry,[32] spectrophotometry,[33] and fluorescence.[34] Nevertheless, more effective and simple methods for AA determination in daily analysis are still high necessary. CDs fluorescent probes has wide application prospect in sensitive and efficient detecting AA among these methods.[35–37]

In this research, an efficient and environmental approach for the preparation of nitrogen- (N) and sulfur- (S) codoped CDs (CDs-IPM) was developed which involved simultaneous addition of BPs derived microcrystalline cellulose (MCC), SO_3H-IL, and polyethylene glycol 400 (PEG 400), respectively. During the process of synthesis, SO_3H-IL functioned as a CDs precursor, N, S dopant, as well as a catalyst for cellulose degradation, while PEG 400 acted as a surface passivating agent. The fabricated CDs-IPM is appropriate for Cr(VI) detection, since it possesses desirable photoluminescence intensity and enhanced physicochemical stability, while its yield following the process of synthesis is also high. Furthermore, the CDs-IPM/Cr(VI) complex system could use as a "turn-on" fluorescence nanoprobe to monitor ascorbic acid (AA) levels. The principle behind the fluorescent "on-off-on" behavior in hexavalent chromium and ascorbic acid determination was comprehensively analyzed. Moreover, the sensitivity, stability, and reproducibility of the CDs-IPM biosensor synthesized in this study were evaluated.

Experimental

Materials

MCC, extracted from liquefied banana pseudo-stem residue according to the method reported previously,[22] was taken as the main carbon source. The SO_3H-IL was prepared based on the procedure described previously.[38] The reagents PEG400, was obtained from Aladdin Biochemical Technology Co. Ltd. (Shanghai, China). The rest of the chemicals were reagent grade, and they did not require purification process.

Methods

One-step hydrothermal preparation of CDs samples. Working from existing hydrothermal methods,[23,39] six different carbon dots were fabricated *via* single-step hydrothermal treatment according to the experimental conditions presented in Table 1. The reactants MCC, SO_3H-IL, and PEG400 were mixed thoroughly with DI water (30 mL), then the resulting reaction mixture was shifted to a Teflon-lined autoclave to allow the reagents to react at 200 °C for 6 h. After removing the black precipitate by centrifugation, the supernatant collected was filtered, purified with a 500 dalton molecular weight cut-off dialysis bag against ultrapure water. The pure carbon dots samples were then freeze-dried for further investigation and use. The synthesis yield (SY) was calculated according to the following formula (1):

$$\mathrm{SY} = (M_{\mathrm{CDs}}/M_{\mathrm{p}}) \times 100\% \quad (1)$$

where M_{CDs} and M_{p} are the mass of the synthesized CDs and charged precursors, respectively.

CDs-IPM plays a fluorescence nanoprobe to estimate Cr(VI) and AA. Fluorescence probe applications of CDs-IPM were carried out using conventional means reported in literature.[20,40] Specifically, to estimate the selectivity of the CDs-IPM probe, aqueous solutions containing different metal ions (Fe^{2+}, Fe^{3+}, Cu^{2+}, Ag^{+}, Co^{2+}, Mg^{2+}, Pb^{2+}, La^{3+}, Al^{3+}, Ca^{2+}, Cd^{2+}, Hg^{2+}, Cr^{3+}, and $Cr_2O_7^{2-}$) and various common anion ions (HCO_3^{-}, $H_2PO_4^{-}$, $S_2O_3^{2-}$, ClO_4^{-}, S^{2-}, F^{-}, Cl^{-}, Br^{-}, I^{-}, SO_4^{2-}, CO_3^{2-}, PO_4^{3-} and NO_3^{-}) were prepared to have a final concentration of 20 μM. The fixed concentration of CDs-IPM in PBS solution (pH 7.4) was 200 μM. The PL intensities were recorded after the addition of the aforesaid ion liquids into the CDs-IPM, the volume fraction of each of ion solution was 9%. To assess the linearity, range as well as the limit of detection (LOD) towards Cr(VI), 20 μL of the ion-solutions with various concentrations of chromium(VI) were blended individually into 180 μL of CDs-IPM. Meanwhile, 20 μL of ultrapure water was taken as a control sample. The concentration variable fluorescence intensity was recorded under the $\lambda_{ex}/\lambda_{em}$ at 397/455 nm. F and F_0 each represent the PL intensity of the CDs-IPM with and without the existence of metal ion.

To monitor the AA levels, 20 μL of the hexavalent chromium (100 μM) was mixed with 200 μL of CDs-IPM solution (100 μg mL^{-1}) to form the CDs-IPM/Cr(VI) probe. Thereafter the fluorescence spectra were measured after 120 μL of AA adding into

Table 1 Experimental conditions of the synthesis process of individual CDs along with their corresponding designations

Codes	MCC/g	SO_3H-IL/g	PEG400/g	NaOH/g
CDs-IP	0	2	5	0
CDs-PM	1	0	5	0
CDs-IPM	1	2	5	0
CDs-IM	1	2	0	0
CD-H	1	0	0	0
CD-A	1	0	0	1.2

the above mixed solution and maintaining for 2 min. To assess the selectance of the CDs-IPM/Cr(VI) sensor towards ascorbic acid, other reducing agents and familiar anions (HCO_3^-, HPO_4^{2-}, $S_2O_3^{2-}$, ClO_4^-, S^{2-}, F^-, Cl^-, Br^-, I^-, SO_4^{2-}, CO_3^{2-}, PO_4^{3-}, and NO_3^-) were utilized using the above-mentioned procedure. To access the range of linearity and the LOD of ascorbic acid, 10 μL of an ascorbic acid liquid at gradient concentrations (0.0–100 μM) was added and the same procedure described above was repeated.

Determination of Cr(VI) and AA in real samples. For the detection of Cr(VI) in environmental water samples, Changqing Lake water (Changqing, Jinan province, China) was used as the actual samples. The water sample was centrifuged, filtered and boiled to remove impurities and residual chlorine. Subsequently, the lake water was detected with the addition of 200 μL different concentrations of Cr(VI) standard solutions to calculate the recovery of Cr(VI). The fluorescence spectra were tested when the above solution were spiked into 2 mL CDs-IPM solution.

For the determination of AA, orange, lemon, pear, strawberry, apple and kiwi were bought from a local supermarket (Changqing, Jinan province, China). These fruits were squeezed, and juicers obtained were then subjected to centrifuged, filtered. After that, the filtered juices were double diluted with the ultrapure water for the further use. PL intensities were measured as mentioned in the previous section. All the samples were tested by three parallel measurements, and fluorescence spectra were measured at room temperature with the excitation and emission wavelengths of 397 nm and 455 nm, respectively.

Characterizations

Fluorescence spectrum of CDs samples were determined using an FL-7000 fluorescence spectrometer (Hitachi, Japan). The excitation increased ranging from 300 to 420 nm by a 20 nm growth. Fluorescence lifetime measurement was conducted on a time-correlated single-photon counting system (FLS 920, Edinburgh Instruments, UK). Atomic force microscopy (AFM) photographs of CDs-IPM were obtained from an atomic force microscope (Bruker, Germany). High-resolution transmission electron microscopy (HR-TEM) observation for CDs was measured by a 200 kV JEOL-2010 (JEOL Ltd., Japan) electron microscope. X-ray photoelectron spectroscopy (XPS) was acquired with an Amicus spectrometer (Shimadzu, Japan). The Fourier transform infrared spectroscopy (FT-IR) was performed in the spectral range of 500 to 4000 cm^{-1} through a Tensor 27 spectrometer (Bruker, Germany). The Raman spectra of the CDs samples were measured on Renishaw RM 2000 (Renishaw, UK) with an argon-ion laser. The ultraviolet-visible (UV-Vis) absorption spectrum was recorded on a UV-3600 spectrometer (Shimadzu, Japan). The quantum yield of the CDs-IPM was calculated taking quinine sulfate (in 100 μM H_2SO_4) as reference by the formula:[41]

$$Q_X = Q_{St} \times (A_X/A_{St}) \times (I_{St}/I_X) \times (\eta_X/\eta_{St})^2 \quad (2)$$

Results and discussion

Optical properties of CDs-IPM

The result of the fluorescence spectrum of the six different carbon dots at the same concentration is presented in Fig. 1. The PL emission of all carbon dots shifted to a longer wavelength with an increase in the exciting wavelength by an increment of 10 nm. The fluorescent emission performance with excitation wavelength-dependence is thought to be involved in the different band gaps of carbon dots in an aqueous solution with different sizes or the lateral sizes of different emissive sites.[24] Additionally, various surface states and surface functional groups of CDs also lead to disparity in emission peak positions.[42] The optimum excitation and corresponding emission wavelengths of the unmodified carbon dots samples are listed in Table S1† and a comparison to their fluorescence spectrum at respective optimal excitation wavelength is displayed in Fig. 1f. The PL intensities of CDs-PM and CDs-H were lower than that of CDs-IM, while the PL intensity of the CDs-A was greatly increased, which might be attributed to the increase in surface defects introduced by oxygen-containing functional groups after alkali treatment.[9] CDs-IP and CDs-IPM had the highest and the second-highest photoluminescence

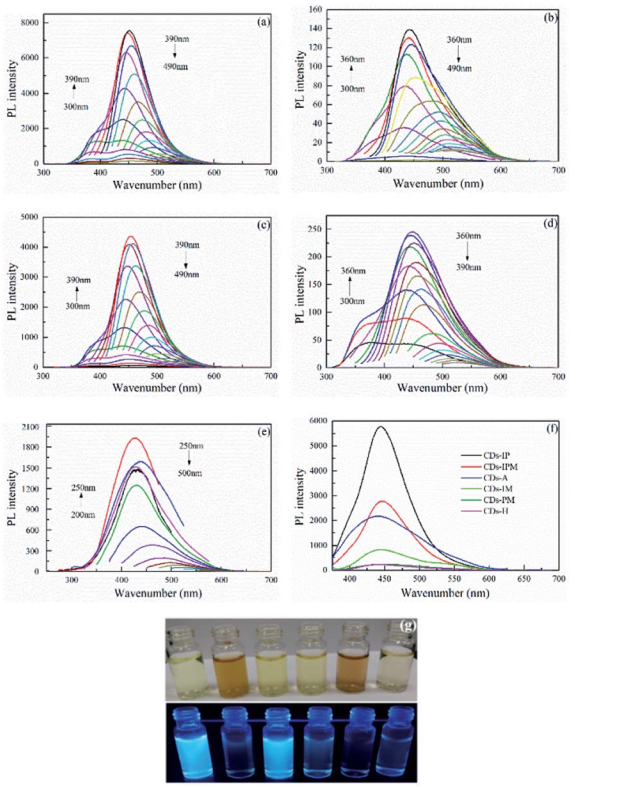

Fig. 1 Fluorescence emission spectra of diluted suspensions of (a) CDs-IP, (b) CDs-PM, (c) CDs-IPM, (d) CDs-IM, and (e) CDs-A, respectively, excited at increasing wavelengths. (f) Comparison of PL intensity for six different CDs at their respective optimal excitation wavelength. (g) Photographs of CDs-IP, CDs-PM, CDs-IPM, CDs-IM, CDs-H, CDs-A suspensions (100 μg mL^{-1}, from left to right) taken in visible and ultraviolet light, respectively.

intensities among them, and PL intensity of CDs-IPM was more than 30 times higher than that of common CDs. Micrographs of the six different CDs aqueous solutions were captured. As evident from Fig. 1g, the color of CDs was light yellow or brown in visible light, while they showed blue fluorescence with distinct brightness in a 365 nm UV lamp. The synthetic yield of the CDs-IPM was the highest compared to all the other CDs samples (Table S1†). The synergistic effect of N, S doping and PEG passivation promoted the fluorescence and SY in the case of CDs-IPM. The SO3H-IL functioned as the CDs precursor, sulfur and nitrogen element provider, additionally contributing to creating surface defects in the CDs, while actively catalyzing the MCC degradation during the hydrothermal process. The addition of PEG400 produced surface passivation and increased oxygen (O)-containing groups on the CDs surface by forming a thin insulating layer, thus enhancing its PL intensity. These attractive properties make CDs-IPM a suitable candidate for further structural and functional investigations.

The optical absorption spectrum of the CDs-IPM have been demonstrated in Fig. 2a, whereby two characteristic absorption bands around 210 nm and 275 nm were found. The absorption bands at 210 nm is attributed to π–π* electronic transition of aromatic π system, and absorption bands at 275 nm is related to n–π* electronic transitions of the C=O band.[11] The interaction between π- and n-states could be seized with the degree of the orbital eclipsing and its electron withdrawal or donation-based capabilities.[15] That is, the optical properties of CDs are influenced orbital eclipsing and its electron withdrawal or donation-based capabilities.[15] That is, the optical properties of CDs are influenced by their underlying electronic structure.[43] It's reported that the presence of vacancies and surface defects in synthesized Cu-doped graphene oxide could affect its photoluminescence characterization.[44] The PL decay experiments for CDs-IPM were performed and the experimental results revealed that the emission followed a single exponential decay (Fig. 2b). The resulting curve was exponential fitted and the average exciton lifetime (τave) of CDs-IPM was calculated using the formula:

$$\tau_{ave} = (A_1\tau_{12} + A_2\tau_{22} + A_3\tau_{32})/(A_1\tau_1 + A_2\tau_2 + A_3\tau_3) \quad (3)$$

in which A_1, A_2 and A_3 represent normalized pre-exponential factors, and τ_1, τ_2 and τ_3 represent typical of representative lifetimes.[45] The photoluminescence lifetime of CDs-IPM was found to be 3.21 ns. The various dynamic behaviors of chemical states heavily influence the heterogeneous electronic structures which is important for the emission-based performance of carbon dots in turn.[10] Hence, it can be speculated that deviations in the PL lifetime of CDs-IPMs might certainly be affected by displaced S, N atoms and S, N- or oxygenic edge functional groups.

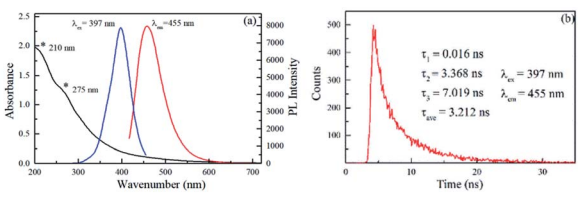

Fig. 2 (a) Ultraviolet absorption spectra, optimum fluorescent excitation and emission spectrum of diluted suspensions of CDs-IPM. (b) Fluorescence decay curve and lifetime of CDs-IPM.

Physicochemical characterization of CDs-IPM sensors

The Fig. 3a represents the scheme of CDs-IPM synthesis based on our preliminary analysis. The CDs-IPM were observed as elliptical or nearly circular nano-dots with size distribution ranging from 1.0 and 4.6 nm under TEM (Fig. 3b). The CDs-IPM has average diameter of approximately 3.3 nm. HR-TEM images of CDs-IPM revealed lattice parameters of 0.21 nm (Fig. 3c), which are representative of the ⟨102⟩ lattice fringe of graphene. AFM images of CDs-IPM [Fig. 3d and e] illustrate that the heights of CDs-IPM were less than 4.0 nm, suggesting that the as-prepared CDs-IPM possesses several layers of graphene (<4 layers).

The composition and chemical bonding state of the carbon dots were investigated by means of XPS measurements. In Fig. 4a, the contrastive XPS spectrum of CDs-A and CDs-IPM have been presented, which demonstrate the presence of O 1s and carbon (C) 1s peaks at 532.41 and 284.83 eV, respectively, while S 2p peak and N 1s peak at 167.89 and 401.61 eV are evident. The elemental analysis of CDs-IPM reveals the presence

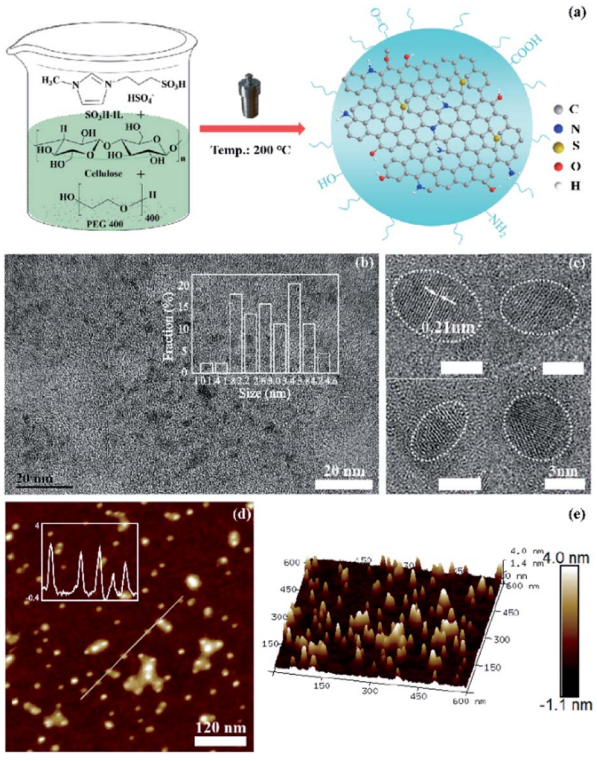

Fig. 3 (a) Graphical representation of the preparation process for the CDs-IPM. (b) and (c) TEM and HR-TEM micrographs of the CDs-IPM, with their corresponding size distribution. (d) and (e) AFM profile of CDs-IPM, with corresponding height profile inset in the micrograph.

of 36.56% of C, 57.87% of O, 2.3% of N, and 3.27% of S. In Fig. 4b, five peaks, including C–C (284.7 eV), C–N (285.2 eV), C–O (286.3 eV), C=O (287.6 eV), and O–C=O (288.6 eV) can be obtain by deconvoluting the high-resolution C1s spectra of the CDs-IPM, which demonstrates the generation of doped N and oxygenic functional groups in the structure.[10] The O1s spectrum has peaks at 531.9 and 531.4 eV (Fig. 4c), which is ascribed to the presence of C–OH/C–O–C and carbonyl groups. And the resolved peaks at 400.0 and 399.5 eV in the N 1s spectra (Fig. 4d) revealed the existence of pyrrolic-N and pyridinic-N.[46] Two peaks, one at 163.9 eV and the other at 165.1 eV, were typically deconvoluted from the high-resolution S2p spectra (Fig. 4e), which is indicative of the existence of sulfur in the form of C–S covalent and oxide S, respectively.

The FT-IR test was conducted to identify the surface functional groups on the CDs-IPM, and the result is presented in Fig. 4f. Corroborating with the XPS results, a broad absorption band was detected around 3356 cm^{-1}, which relative to the stretching vibration of N–H and O–H.[21] The presence of the C–H bond is confirmed by the peaks observed at 2959 and 2873 cm^{-1}, and the stretching vibration of C–O–C or C=C groups result in the peak appeared at 1633 cm^{-1}.[18] Peaks at 1570, 1461 and 1383 cm^{-1} illustrate the presence of aromatic heterocyclic C–C and C–N compounds.[47] Additionally, the absorption bands at 1062–1111 cm^{-1} can be related to the presence of C–O, C–S, and C–O–C bonds.[46] The XPS and FT-IR analysis results confirmed that the sulfur and nitrogen atoms and the oxygenic groups were successfully introduced into the unmodified CDs-IPM. The co-doped N and S endowed the CDs-IPM with individual chemical bonds and disordered structures (in forms of N, S hybridized atoms and vacancy defects) in the graphene lattice, where the two types of hybridized (sp^2 and sp^3) carbon atoms were ubiquitous.[23]

The Raman spectra in Fig. 4g confirmed that the disorder in the carbon-skeleton was attributed to the existence of a defective or disordered peak at 1332 cm^{-1} (D-band) and a graphitic peak at 1572 cm^{-1} (G-band). The D band intensity of CDs-IPM was stronger than that of CDs-A. The D band is attributed to carbon atoms exist in the disordered carbon structure, and the G band is ascribed to the C sp^2 in the 2D hexagonal lattice of a graphite cluster.[43] Therefore, the effects of doping and strain may account for the variation in the Raman spectra.[48]

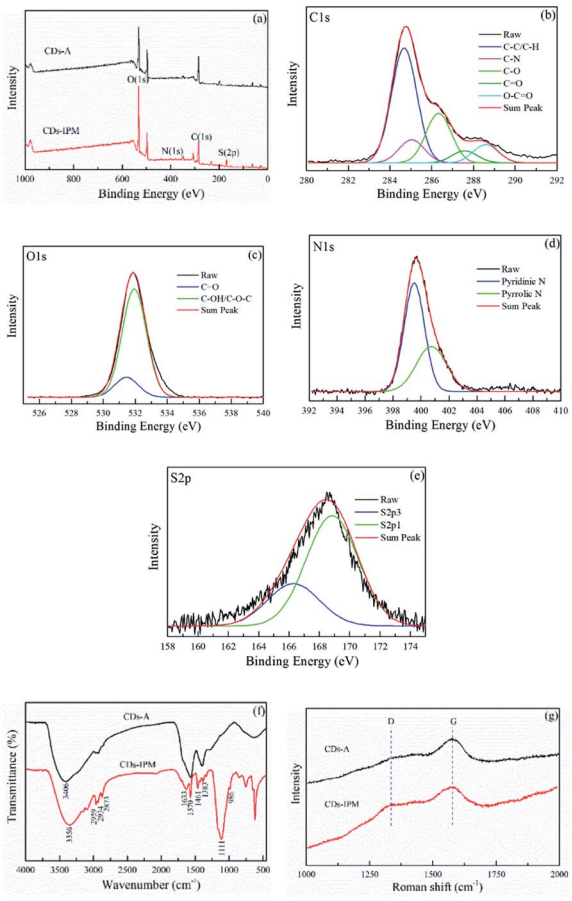

Fig. 4 (a) Comparative XPS spectrum towards two different carbon dots, and high-resolution X-photoelectron spectroscopy analysis for (b) C1s peak, (c) O1s peak, (d) N1s peak, and (e) S2p peak, respectively. (f) FT-IR spectrum of CDs-IPM. (g) Raman spectrum of two different carbon dots.

The sensing behavior of the CDs-IPM sensing system

The selectivity of the CDs-IPM system towards common metal cations was examined, and the results have been provided in Fig. 5a. The addition of hexavalent chromium caused the PL intensity of CDs-IPM a drastic decrease, while other metal ions showed negligible effects, supporting our preliminary hypothesis that hexavalent chromium could selectively lead to fluorescence quenching of the CDs-IPM.

The addition of Fe^{2+}, Fe^{3+}, Cu^{2+}, Ag^{+}, Co^{2+}, Mg^{2+}, Pb^{2+}, La^{3+}, Al^{3+}, Ca^{2+}, CDs^{2+}, Hg^{2+}, and Cr^{3+} into a CD-IPM solution without hexavalent chromium led to negligible changes in fluorescence (Fig. 5b). This result supports our observation in Fig. 5a, wherein we concluded that ions apart from hexavalent

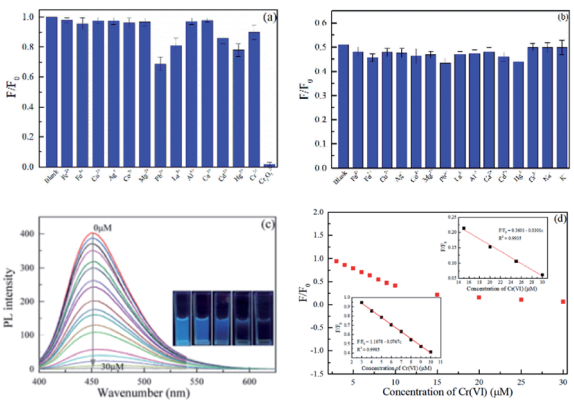

Fig. 5 (a) Relative PL intensities of CDs-IPM with the addition of various metal ions. (b) Effect of different coexistence metal ions on selectivity of Cr(VI) by the synthesized CDs-IPM [each of ion concentration: 5 μM; blank sample consisted of Cr(VI)]. (c) PL emission spectrum of CDs-IPM with the existence of Cr(VI) at different concentrations. (d) The functional relationships of F/F_0 *versus* concentration of Cr(VI).

chromium have no influence on the fluorescence of the synthesized CD-IPMs. The sensitivity of CDs-IPM for Cr(VI) was then evaluated by assessing its concentration-dependent fluorescence intensity. As evident in Fig. 5c, the PL intensities of CDs-IPM systematically decreased with increasing in the concentration of hexavalent chromium in the range of 0 to 30 μM, which was accompanied by a gradual variation in color of the CDs-IPM solution as observed under ultraviolet radiation (bottom right inset in Fig. 5c). Insets in Fig. 5d reveal the dependence of F/F_0 *versus* the concentration of hexavalent chromium. In the given concentration region, two linear relationships (0.25–10 and 15–30 μM) of F/F_0 *versus* concentration of hexavalent chromium were detected. The LOD was as low as 17 nM at a signal-to-noise ratio (S/N) of 3, which could bear comparison with values in previously work. Compared with the method for Cr(VI) detection reported in the literature, the sensing property of the CDs-IPM is more favorable, giving feasibility in real sample analysis (Table S2†). It is worth noting that the LOD of hexavalent chromium in our system is lower than that of maximum allowable level of Cr(VI) discharge of 50 mg L^{-1} in potable water in accordance with the World Health Organization (WHO).[49] Thus, it is reasonable to propose that the CDs-IPM-based system reported in this study is appropriate for Cr(VI) detection in real samples for quality monitoring.

AA can act as a reductant to wipe off Cr(VI) under moderate circumstances.[34] The selectivity, susceptibility to interference, and sensitivity of the CDs-IPM/Cr(VI) complex to AA were also studied. The influence of other reducing agents and familiar anions, such as HCO_3^-, HPO_4^{2-}, $S_2O_3^{2-}$, ClO_4^-, S^{2-}, F^-, Cl^-, Br^-, I^-, SO_4^{2-}, CO_3^{2-}, PO_4^{3-}, and NO_3^- on the CDs-IPM/Cr(VI) fluorescence restoration were explored under the same experimental conditions. In Fig. 6a, AA is the only candidate that showed the potential for revitalizing of the luminescence property of CDs-IPM/Cr(VI) system, among all the other reducing agents investigated, signifying that the "off-on" detection was exclusive to AA. Additionally, the co-existing of these anions brought trifling impact with the fluorescence increase of CDs-IPM/Cr(VI) complex (Fig. 6b). Fig. 6c shows the PL intensity of the original CDs-IPM/Cr(VI) complex to be low, while after gradual introduction of AA (0.0–100 μM), a dose-dependent change in PL intensity of the hybrid was found.

In the specified concentration interval, the recovery of the PL intensity by AA can be described by the following equations:

$$F/F_0 = 1.503 + 0.0064c \ (R^2 = 0.9972) \ (4–15\ \mu M) \quad (4)$$

$$F/F_0 = -0.5352 + 0.1183c \ (R^2 = 0.9975) \ (20–45\ \mu M) \quad (5)$$

$$F/F_0 = -8.6179 + 0.2793c \ (R^2 = 0.9707) \ (50–75\ \mu M) \quad (6)$$

In the above-mentioned equations, F and F_0 represent the PL intensities of CDs-IPM excited at 397 nm with and without addition of AA, respectively. In light of measuring data, the LOD of the CDs-IPM/Cr(VI) ensemble for AA was 103 nM.

Fig. S1† manifests that the PL intensity of the CDs-IPM is reversible during the sequential alternate introduction of Cr(VI) (20 μM) and AA (20 μM), respectively. Although the accumulated Cr(VI) or AA can cause fatigue effects, distinct fluorescence-based changes for sensing Cr(VI) and AA were evident even after five consecutive repeat cycles. This suggests that the fluorescent switch-off or switch-on can be selectively achieved by the Cr(VI) or AA, and the fabricated CDs-IPM can find applications as a recoverably versatile fluorescent-based sensing system.

Detection of Cr(VI) and AA in real samples

The versatile CDs-IPM based fluorescent probe promoted us to further evaluate its detection behavior in real water samples. The fluorescence intensity of lake sample with fixed CDs-IPM added decreased with increasing the concentration of Cr(VI), meanwhile, two good linear relationships were fitted from 0.5 to 18 μM (Fig. S3†). The recovery of Cr(VI) ranged from 98.4–106% with the relative standard deviation (RSD) < 2% ($n = 3$) (Table 2). These results show that the CDs-IPM can be applied to the practical Cr(VI) determination.

Based on the above experimental method, orange, lemon, pear, strawberry, apple and kiwi were choosen as the detection of objects, the AA content of them were determined and calculated by using eqn (4) or eqn (5) in Fig. 6. The RSDs of all the samples were between 0.31% and 1.68% (Table 3), indicating the present CDs-IPM/Cr(VI) system can be an sensor for the detection of AA for real samples

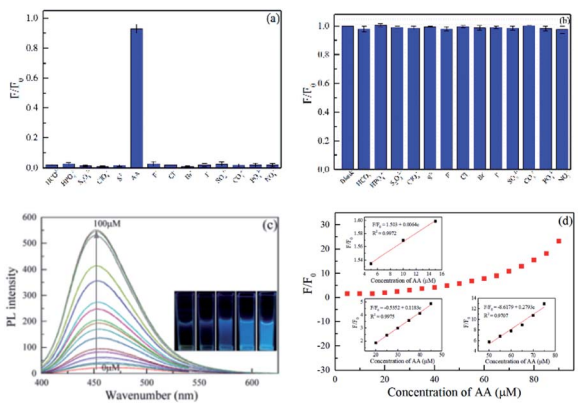

Fig. 6 (a) Fluorescence response for CDs-IPM/Cr(VI) with addition of anions. (b) Effect of different coexistence of anions on AA in the CDs-IPM/Cr(VI) ensemble [5 μM Cr(VI) was the blank with the concentrations of AA and other anions set at 20 μM and 5 μM, respectively]. (c) PL emission spectrum of the CDs-IPM/Cr(VI) system with the existence of AA. (d) The functional relationships between F/F_0 and AA concentration.

Table 2 Recovery of Cr(VI) in Changqing lake water sample ($n = 3$)

Sample	Added Cr(VI) (μM)	Detected Cr(VI) (μM)	Recovery (%)	RSD (%)
1	0.5	0.53 ± 0.04	106 ± 8	0.38
2	5	4.92 ± 0.16	98.4 ± 3.2	0.47
3	10	9.87 ±0.21	98.7 ± 2.1	1.72

Table 3 Determination of AA in fruit ($n = 3$)

Sample	Content of AA (mg/100 g)	Calculating formula	RSD (%)
Orange	41.64	(5)	1.49
Lemon	37.35	(5)	0.76
Pear	4.06	(4)	0.31
Strawberry	28.81	(5)	0.92
Apple	5.72	(4)	0.34
Kiwi	43.93	(5)	1.68

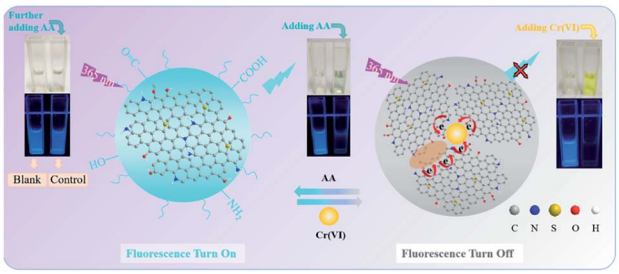

Fig. 7 Schematic illustration of the proposed fluorescence quenching principle for the CDs-IPM/Cr(VI) system.

Possible mechanism for enhanced PL-based performance of the CDs-IPM

Although the veritable mechanism of fluorescent carbon dots is remain strongly debated, it has been confirmed that the photophysical performances of CDs rely on the HOMO–LUMO energy gap, and the heteroatomic doping could tune the PL bandgap through expanding the conjugated field of the fluorophores.[48] The N and S atoms with many lone pair electrons lead to the availability of multiple isolated sp^2 conjugated carbon clusters. And isolated sp^2 conjugated carbon clusters can serve as valid radial centers enhancing the fluorescent performances of the CDs-IPM.

To investigate the "on-off-on" sensing mechanism of CDs-IPM, studies involving the UV-Vis spectrum of hexavalent chromium solution, as well as excitation and emission spectrum of CDs-IPM were performed (Fig. S2a†). The excitation band of CDs-IPM at 397 nm was partly overlapped by the absorption band of hexavalent chromium at 360 nm. Nevertheless, the emission center ($\lambda_{em} = 455$ nm) occupying the longer wavelength region was scarcely influenced, since the extinction coefficient of hexavalent chromium solution around 455 nm is small, suggesting that fluorescence resonance energy transfer (FRET) may be the main quenching mechanism of this system. Although previous studies reported that PL emissions of most CDs can be potentially quenched by hexavalent chromium by virtue of the inner filter effect (IFE),[19,34,50] there is a possibility that the CDs-IPM reported in this study may be potentially different. To figure out the substantive theory, the photoluminescence decay curves of the CDs-IPM with and without the existence of hexavalent chromium were examined. CDs-IPM has a lifetime of about 3.21 ns at 455 nm, while a decrease in the lifetime (2.07 ns at 455 nm) was observed after the addition of hexavalent chromium (Fig. S2b†). Therefore, it is almost certain that the FRET process among the CDs-IPM and hexavalent chromium changes the donor's excitation lifetime. Furthermore, the addition of AA into the CDs-IPM-Cr(VI) complex may also result in the re-establishment of the average lifetime (3.14 ns) of the CDs-IPM.

Fig. 7 describes the probable quenching and recovery principle of the CDs-IPM/Cr(VI) system. It is the non-radiative electron transfer and strengthened interactions in the CDs-IPM/Cr(VI) system that quenched the fluorescence of CDs-IPM (switched off) (Fig. 7 right). Some O-containing groups present in the CDs-IPM may coordinate with the Cr(VI) to form complexes; while the doping of N, S atoms into the graphite-like structure of CDs could potentially modulate its electron density which would facilitate the coordination effect.[51] Thereafter, the CDs-IPM/Cr(VI) complex is dissociated following the addition of ascorbic acid due to the efficient affinity effect of the functional groups present in ascorbic acid.

Besides, hexavalent chromium might be reduced to trivalent chromium by ascorbic acid, and the coordination effect was eliminated.[34,36] In these cases, the subsequent re-dispersion of CDs-IPM restores the fluorescence (switched on) (Fig. 7 left).

The long-term photostability of CDs-IPM sensors

The chemical sensor-based stress resistance is high in environment-based applications. In this study, the effects of pH, NaCl concentrations (from 0 to 1 M), and duration of UV light (365 nm)-based irradiation on the PL of CDs-IPM were studied. Fig. S4a† shows that CDs-IPM can withstand changes across a wide pH range (2–9), which may be due to the variation in the surface functional group of the CDs-IPM. Fig. S4b† indicates the high photostability of CDs-IPM-based sensors in high salt conditions. Moreover, the fluorescence intensity of CDs-IPM only showed slight decrease during prolonged exposure to 365 nm UV lamp, with an irradiation time of 160 min (Fig. S4c†), illustrating the resistance of CDs-IPM to photobleaching. These results demonstrate that CDs-IPM have a robust long-term detection capacity for hexavalent chromium, which is resistant to interference from complex environmental conditions. In comparison with other CDs-based sensors reported previously (Table S2†), the linear range of our method is satisfactory with additional advantages like lower LOD and higher PLQY.

Conclusions

A simple method to prepare N, S codoped bio-based CDs was developed in this study. The synergistic effect of MCC, SO_3H-IL, and PEG 400 during the synthesis process endowed the unmodified CDs-IPM with high synthetic yield, desirable PL intensity, and superior PLQY-based properties. The obtained CDs-IPM were sensitive to Cr(VI), detecting the metal at levels as low as 17 nM. The CDs-IPM–Cr(VI) complex can also be applied as a sensor for AA determination (LOD: 103 nM). Our results demonstrate that the superior fluorescence property and reversible switching behavior of the CDs-IPM are mainly

attributed to the efficient electron transfer between probe and analytes, after the synchronous introduction of N, S atoms and O-containing groups. The unmodified CDs-IPM synthesized in this study can function across a wide pH range and possesses outstanding photostability and excellent long-term fluorescence stability. These distinct properties make this CDs-IPM/Cr(VI)-based "turn-off" fluorescent probe a promising candidate for potential applications in analytical detection and environmental monitoring.

Conflicts of interest

The authors declare that they have no known competing financial interests or personal relationships that could have appeared to influence the work reported in this paper.

Acknowledgements

This research was supported by the National Natural Science Foundation of China (21978059). Also, it was financially supported by the Natural Science Foundation of Shandong Province (ZR2020QB193), Outstanding Youth Innovation Team Project of Shandong Provincial University (2019KJC014), as well as Major Technology Innovation Projects of Shandong Province (2019JZZY010407).

References

1 E. M. Hamilton, S. D. Young, E. H. Bailey and M. J. Watts, *Food Chem.*, 2018, **250**, 105–112.
2 M. Aqeel, M. Ikram, A. Asghar, A. Haider, A. Ul-Hamid, M. Naz, M. Imran and S. Ali, *Appl. Nanosci.*, 2020, **10**, 2045–2055.
3 M. Ikram, J. Hassan, A. Raza, A. Haider, S. Naz, A. Ul-Hamid, J. Haider, I. Shahzadi, U. Qamar and S. Ali, *RSC Adv.*, 2020, **10**, 30007–30024.
4 M. Ikram, A. Raza, M. Imran, A. Ul-Hamid, A. Shahbaz and S. Ali, *Nanoscale Res. Lett.*, 2020, **15**, 95.
5 D. Yoo, Y. Park, B. Cheon and M.-H. Park, *Nanoscale Res. Lett.*, 2019, **14**, 272.
6 G. Wang, S. Zhang, J. Cui, W. Gao, X. Rong, Y. Lu and C. Gao, *Anal. Chim. Acta*, 2022, **1195**, 339478.
7 H. Zhang, Y. Huang, Z. Hu, C. Tong, Z. Zhang and S. Hu, *Microchim. Acta*, 2017, **184**, 1547–1553.
8 X. Lin, M. Xiong, J. Zhang, C. He, X. Ma, H. Zhang, Y. Kuang, M. Yang and Q. Huang, *Microchem. J.*, 2021, **160**, 105604.
9 F. Yuan, Z. Wang, X. Li, Y. Li, Z. a. Tan, L. Fan and S. Yang, *Adv. Mater.*, 2017, **29**, 1604436.
10 K. Jiang, L. Zhang, J. Lu, C. Xu, C. Cai and H. Lin, *Angew. Chem., Int. Ed.*, 2016, **55**, 7231–7235.
11 J. Tan, Q. Li, S. Meng, Y. Li, J. Yang, Y. Ye, Z. Tang, S. Qu and X. Ren, *Adv. Mater.*, 2021, **33**, 2006781.
12 S. Sun, Q. Chen, Z. Tang, C. Liu, Z. Li, A. Wu and H. Lin, *Angew. Chem., Int. Ed.*, 2020, **59**, 21041–21048.
13 J. Li, S. Yang, Z. Liu, G. Wang, P. He, W. Wei, M. Yang, Y. Deng, P. Gu, X. Xie, Z. Kang, G. Ding, H. Zhou and X. Fan, *Adv. Mater.*, 2021, **33**, 2005096.
14 A. Alaghmandfard, O. Sedighi, N. Tabatabaei Rezaei, A. A. Abedini, A. Malek Khachatourian, M. S. Toprak and A. Seifalian, *Mater. Sci. Eng. C*, 2021, **120**, 111756.
15 M. Shaker, R. Riahifar and Y. Li, *FlatChem*, 2020, **22**, 100171.
16 M. Kurian and A. Paul, *Carbon Trends*, 2021, **3**, 100032.
17 L. Wang, W. T. Li, B. Wu, Z. Li, S. L. Wang, Y. Liu, D. Y. Pan and M. H. Wu, *Chem. Eng. J.*, 2016, **300**, 75–82.
18 S. Sawalha, A. Silvestri, A. Criado, S. Bettini, M. Prato and L. Valli, *Carbon*, 2020, **167**, 696–708.
19 M. Athika, A. Prasath, E. Duraisamy, V. Sankar Devi, A. Selva Sharma and P. Elumalai, *Mater. Lett.*, 2019, **241**, 156–159.
20 X. Yang, J. Xu, N. Luo, F. Tang, M. Zhang and B. Zhao, *Food Chem.*, 2020, **310**, 125832.
21 A. Paul and M. Kurian, *Mater. Today: Proc.*, 2020, **25**, 213–217.
22 F. Meng, X. Zhang, W. Yu and Y. Zhang, *Ind. Crops Prod.*, 2019, **137**, 377–385.
23 L. Ansari, S. Hallaj, T. Hallaj and M. Amjadi, *Colloids Surf. B: Biointerfaces*, 2021, **203**, 111743.
24 F. Yan, Y. Jiang, X. Sun, Z. Bai, Y. Zhang and X. Zhou, *Microchim. Acta*, 2018, **185**, 424.
25 H. Zhang, B. Wang, X. Yu, J. Li, J. Shang and J. Yu, *Angew. Chem., Int. Ed.*, 2020, **59**, 19390–19402.
26 M. Ikram, M. I. Khan, A. Raza, M. Imran, A. Ul-Hamid and S. Ali, *Phys. E Low-dimens. Syst. Nanostruct.*, 2020, **124**, 114246.
27 M. Ikram, R. Tabassum, U. Qumar, S. Ali, A. Ul-Hamid, A. Haider, A. Raza, M. Imran and S. Ali, *RSC Adv.*, 2020, **10**, 20559–20571.
28 M. Ikram, J. Hassan, M. Imran, J. Haider, A. Ul-Hamid, I. Shahzadi, M. Ikram, A. Raza, U. Qumar and S. Ali, *Appl. Nanosci.*, 2020, **10**, 3525–3528.
29 A. Raza, J. Z. Hassan, M. Ikram, S. Naz, A. Haider, A. Ul-Hamid, I. Shahzadi, J. Haider, S. Goumri-Said, M. B. Kanoun and S. Ali, *Surface. Interfac.*, 2021, **27**, 101571.
30 M. Nafees, M. Ikram and S. Ali, *Appl. Nanosci.*, 2017, **7**, 399–406.
31 M. Malik, V. Narwal and C. S. Pundir, *Process Biochem.*, 2022, **118**, 11–23.
32 X. Xu, C.-H. Li, H. Zhang and X.-M. Guo, *Nanomaterials*, 2022, 12.
33 N. V. Saranchina, A. A. Damzina, N. A. Gavrilenko, T. N. Volgina, Y. E. Ermolaev, M. S. Polonskaya and M. A. Gavrilenko, *Mendeleev Commun.*, 2022, **32**, 136–138.
34 X. Gong, Y. Liu, Z. Yang, S. Shuang, Z. Zhang and C. Dong, *Anal. Chim. Acta*, 2017, **968**, 85–96.
35 Y. Ji, X. Zou, W. Wang, T. Wang, S. Zhang and Z. Gong, *Microchem. J.*, 2021, **167**, 106284.
36 D. Wang, L. Zhang, P. Li, J. Li and C. Dong, *New J. Chem.*, 2020, **44**, 20806–20811.
37 X. Luo, W. Zhang, Y. Han, X. Chen, L. Zhu, W. Tang, J. Wang, T. Yue and Z. Li, *Food Chem.*, 2018, **258**, 214–221.
38 Y. Liu, W. Xiao, S. Xia and P. Ma, *Carbohydr. Polym.*, 2013, **92**, 218–222.
39 C. He, P. Xu, X. Zhang and W. Long, *Carbon*, 2022, **186**, 91–127.
40 W.-K. Li, J.-T. Feng and Z.-Q. Ma, *Carbon*, 2020, **161**, 685–693.

41 M. Jia, L. Peng, M. Yang, H. Wei, M. Zhang and Y. Wang, *Carbon*, 2021, **182**, 42–50.
42 X. Li, S. Zhao, B. Li, K. Yang, M. Lan and L. Zeng, *Coord. Chem. Rev.*, 2021, **431**, 213686.
43 B. J. Moon, D. Jang, Y. Yi, H. Lee, S. J. Kim, Y. Oh, S. H. Lee, M. Park, S. Lee and S. Bae, *Nano Energy*, 2017, **34**, 36–46.
44 M. Ikram, S. Ali, M. Aqeel, A. Ul-Hamid, M. Imran, J. Haider, A. Haider, A. Shahbaz and S. Ali, *J. Alloys Compd.*, 2020, **837**, 155588.
45 H. Zheng, Z. Jiang, H. Zhai, Z. Zheng, P. Wang, Z. Wang, Y. Liu, X. Qin, X. Zhang and B. Huang, *Appl. Catal. B Environ.*, 2019, **243**, 381–385.
46 W. Zhou, J. Zhuang, W. Li, C. Hu, B. Lei and Y. Liu, *J. Mater. Chem. C*, 2017, **5**, 8014–8021.
47 X. Luo, W. Zhang, Y. Han, X. Chen, L. Zhu, W. Tang, J. Wang, T. Yue and Z. Li, *Food Chem.*, 2018, **258**, 214–221.
48 Y. Wang, Y. Li and L. Feng, *J. Phys. Chem. Lett.*, 2020, **11**, 10439–10445.
49 U. S. E. P. A. (EPA), 2012, **http://water.epa.gov/drink/info/chromium/**.
50 V. Roshni, S. Misra, M. K. Santra and D. Ottoor, *J. Photochem. Photobiol. Chem.*, 2019, **373**, 28–36.
51 L. Li, B. Yu and T. You, *Biosens. Bioelectron.*, 2015, **74**, 263–269.